Evaluation of the Role of Tumor-Associated Macrophages in an Experimental Model of Peritoneal Carcinomatosis Using ^{18}F-FDG PET

Lucia Cottone[*1,2], Silvia Valtorta[*3–6], Annalisa Capobianco[1], Sara Belloli[3,4,6], Patrizia Rovere-Querini[7], Ferruccio Fazio[3,6], Angelo A. Manfredi[1,2], and Rosa Maria Moresco[3,4,6]

[1]Autoimmunity and Vascular Inflammation Unit, San Raffaele Scientific Institute, Milan, Italy; [2]Università Vita-Salute San Raffaele, Milan, Italy; [3]Nuclear Medicine Department and PET Centre, San Raffaele Scientific Institute, Milan, Italy; [4]IBFM, CNR, Milan, Italy; [5]Fellowship of the Doctorate School of Molecular Medicine, University of Milan, Milan, Italy; [6]Tecnomed Foundation, Foundation of University of Milano-Bicocca, Milan, Italy; and [7]Unit of Innate Immunity and Tissue Remodelling, San Raffaele Scientific Institute, Milan, Italy

PET is widely used at the clinical and preclinical levels for tumor assessment and evaluation of treatment efficacy. Here, we established and took advantage of a preclinical model of peritoneal carcinomatosis to evaluate the contribution of inflammatory infiltrating macrophages in tumor progression that was followed using ^{18}F-FDG PET. **Methods:** Groups of mice with peritoneal carcinomatosis were longitudinally evaluated with ^{18}F-FDG PET. Intraperitoneal depletion of macrophages was achieved by an approach (i.e., administration of clodronate encapsulated into liposomes) that proved to be safe and effective. Sham liposomes were used in control animal cohorts. **Results:** ^{18}F-FDG PET allowed us to detect and monitor peritoneal lesion growth and diffusion. Macrophage-depleted animals showed a substantial reduction in tumor burden paralleled by a decrement in the extent of radioactivity distribution. A significant correlation between lesion dimension and metabolic volume was observed not only in macrophage-depleted but also in sham-treated mice. **Conclusion:** ^{18}F-FDG PET allowed a noninvasive detection of peritoneal carcinomatosis lesions. Although macrophages play a key role in the early growth and spreading of lesions in the peritoneal cavity, neoplastic cells apparently represent the major player in this system in the uptake of ^{18}F-FDG.

Key Words: peritoneal carcinomatosis; macrophages; ^{18}F-FDG PET; clodronate; inflammation

The propagation of neoplastic cells in the peritoneal cavity onto parietal or visceral peritoneal surfaces causes peritoneal carcinomatosis, which presents as malignant ascites, multiple small neoplastic nodules, multiple masses of various sizes, and multiple layers of confluent tissue that envelop the serosal surfaces and peritoneal organs. Primary cancers of the peritoneum, such as primary peritoneal carcinoma and peritoneal mesothelioma, are rare. However, secondary carcinomatosis of ovarian, gastric, pancreatic, colorectal, and appendiceal carcinoma origin is relatively common, affecting up to 19% of patients after curative resection of carcinoma and 23%–29% of patients with gastric cancer (1,2). Implantation of neoplastic clusters depends on adhesion molecules expressed on transformed cells. Moreover, neoplastic cells are dispersed in peritoneal lymphatic and venous vessels, and surgical resection possibly further fosters lesion spreading, because healing of injured tissues leads to entrapment of neoplastic cells (3).

Molecular imaging and PET-based techniques in particular represent essential tools for stratification of neoplastic patients and follow-up after treatment (4). ^{18}F-FDG has been extensively used for staging and diagnosis of recurrent ovarian cancer and for the detection of peritoneal carcinomatosis (5). The recent availability of dedicated small-animal tomographs has enabled the in vivo monitoring of lesions in preclinical settings using protocols already applied in clinical practice (6,7). So far, ^{18}F-FDG PET has been used in a limited number of studies to monitor traditional or innovative therapies for peritoneal cancer (8).

Solid tumors comprise malignant cells, resident stromal cells, and infiltrating inflammatory leukocytes. Among them, tumor-associated macrophages, referred to as TAMs, are blood-borne phagocytes that release many factors involved in the remodelling of the extracellular matrix and formation of new blood vessels (9). Peritoneal inflammatory lesions are extensively infiltrated by activated macrophages (10,11), which possibly contribute to the development and growth of neoplastic masses (12).

The aim of this study was to assess the role of inflammatory macrophages in peritoneal carcinomatosis, using ^{18}F-FDG PET to monitor in vivo tumor progression and diffusion.

To address this issue, we set up an experimental model of peritoneal carcinomatosis based on the intraperitoneal

injection of murine syngeneic TS/A adenocarcinoma cells (13).

We have evaluated the extent of peritoneal involvement and the uptake of ^{18}F-FDG before or after depletion of phagocytes using clodronate—a drug able to kill activated macrophages—encapsulated into liposomes (14). Because ^{18}F-FDG is known to accumulate also in nonneoplastic cells that infiltrate the neoplasm, the study was designed also to better address the relative contribution of inflammatory macrophages and proliferating carcinoma cells in ^{18}F-FDG PET images.

MATERIALS AND METHODS

Mice

BALB/C female mice (6–7 wk of age) were purchased from Charles River. Animals were kept under specific pathogen-free conditions and were handled and maintained according to our Institutional Animal Care and Use Committee ethical regulations. At the end of experiments, animals were sacrificed by CO_2 asphyxiation.

Cells and Tumor Analysis

TS/A is a murine spontaneous mammary adenocarcinoma line originated in BALB/C mice (13). Cells were grown in RPMI (Gibco BRL) containing 10% fetal bovine serum (South American origin; BioWhittaker-Lonza), 2 mM glutamine, penicillin (100 IU/mL), and streptomycin (100 g/mL) (Gibco BRL). Cells were routinely tested for *Mycoplasma* using a MycoAlert mycoplasma detection kit (BioWhittaker-Lonza). Tumor lesions were microdissected and either processed for immunohistochemistry or, when indicated, dehydrated to assess their net weight.

Study Design

BALB/C mice were intraperitoneally implanted with TS/A adenocarcinoma cells (4×10^5 cells/mouse). The dose represents the minimum tumor dose that elicited the growth of neoplastic lesions in 100% of animals, as determined in preliminary experiments (data not shown). First, we performed a model-setting study ($n = 4$) to evaluate the feasibility of ^{18}F-FDG PET to monitor onset and progression of peritoneal carcinomatosis, then a longitudinal study ($n = 12$) to evaluate disease progression in macrophage-competent or -depleted mice, and finally single-point studies ($n = 20$) focusing on obtained data. In the model-setting study, ^{18}F-FDG PET was performed at 4 and 10 d after TS/A adenocarcinoma cell inoculation; the day after the last PET acquisition, animals were sacrificed for histologic analysis. For the longitudinal and the single-point studies, mice were divided in 2 groups and treated intraperitoneally with either dichloromethylenebisphosphonic acid (clodronate; 1 mg of clodronate/20 mg of body weight in 200 μL of suspension), to deplete macrophages, or phosphate-buffered saline encapsulated into liposomes (Clodrolip and Shamlip, respectively) prepared as described (14) and purchased from http://clodronateliposomes.org. Treatments were administered at 6 h after TS/A adenocarcinoma cell injection and consistently (at days 2, 5, 8, and 11 after TS/A adenocarcinoma cell inoculation) until the end of the study (Fig. 1). In the longitudinal study, mice were evaluated using ^{18}F-FDG PET at 5, 7, 9, and 12 d after cell inoculation and sacrificed the day after the last PET acquisition. Additional groups of mice (single-point study) were evaluated using PET at 7 or 12 d and sacrificed at 8 and 13 d after TS/A adenocarcinoma cell inoculation, respectively (Fig. 1). At the moment of necropsy, 1 mouse per cohort was used for immunohis-tochemical analysis; the other mice were used for the assessment of lesion weight (longitudinal and single-point studies).

PET Studies

^{18}F-FDG is routinely prepared in our facility for clinical use (European Pharmacopoeia VII ed.) and it was injected with a radiochemical purity greater than 99%. In vivo imaging studies were performed using a small-animal tomograph, the YAP-(S)-PET II (I.S.E. s.r.l.). After a slight anesthesia with ether, animals were injected in the tail vein with 4.3 ± 0.3 MBq of ^{18}F-FDG in a volume of 50 μL of saline. Immediately before PET acquisition, mice were anesthetized with isoflurane (isoflurane/air 1:1) and positioned prone on the tomograph bed with the abdomen centered in the tomograph field of view (FOV). PET scans started 60 min after tracer injection and lasted for 30 min (6 frames of 5 min each). PET data were acquired in list mode using the full axial acceptance angle of the scanner (3-dimensional mode) and then reconstructed with the expectation maximization algorithm (15).

Image Analysis

A visual inspection analysis was initially applied to PET images to verify the feasibility of ^{18}F-FDG PET in monitoring growth and diffusion of peritoneal carcinomatosis and the effect of macrophage depletion on tracer uptake. Adjacent transaxial ^{18}F-FDG–positive slices, depending on the presence of abnormal areas of radioactivity accumulation, were selected. Images were also quantified using ImageJ (16) and MatLab (MathWorks Inc.) software to obtain the following parameters: maximum ^{18}F-FDG uptake in lesions expressed as maximum standardized uptake value (SUV); mean ^{18}F-FDG uptake in lesions expressed as mean SUV; and extent of ^{18}F-FDG uptake areas expressed as tumor volume (cm^3).

To this aim, PET images were calibrated to transform count per voxel values in MBq/g and corrected for ^{18}F half-life (108.9 min). Volumes of radioactivity accumulation were automatically extracted (mask) using ImageJ software following the definition of threshold values. This procedure has the advantage of avoiding operator-dependent selections of the volume of increased tracer uptake, although it may be affected by partial-volume-effect artifacts, particularly in the case of small regions or radioactivity concentration values close to background level. To automatically extract lesion from background radioactivity or nonspecific uptake present in the urinary bladder, upper and lower threshold values were selected from each mouse PET study. Upper values were identified by centering a circular region of interest (mean area, 11 mm^2) on the maximum value of radioactivity uptake present in the abdominal region. Upper values were selected to avoid urinary bladder uptake that is higher than that present in lesions (data not shown). Lower values were then defined as the double value of radioactivity concentration measured by drawing a circular region of interest (mean area, 7 mm^2) on a thorax muscle. The use of thorax muscle instead of abdominal background was previously set up and validated in a group of normal mice. The validation of this procedure was necessary to verify that thresholded maps extracted did not include gastrointestinal activity. Using the thresholds above, we automatically extracted lesion masks for each PET study using MatLab software. Mean and maximum uptake $\pm$ SD of radioactivity concentration expressed in MBq/g and the number of voxels with radioactivity values included in the identified threshold range were automatically calculated. Finally, radioactivity concentration values were transformed into SUVs by correcting for mouse weights (SUV), and number of voxels was
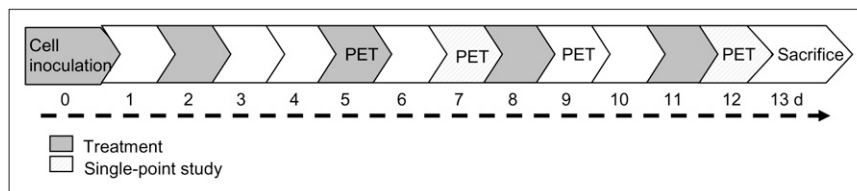
FIGURE 1. Schematic representation of study design.

Histologic Analysis and Flow Cytometry

After sacrifice, tumor lesions were dissected, fixed in 4% paraformaldehyde, cryopreserved in liquid N_2–cooled isopentane, and embedded in optimal cutting temperature compound (Killik; Bio-Optica). Serial 6-μm-thick sections were treated with 0.3% H_2O_2 to quench endogenous peroxidase activity. To evaluate leukocyte and macrophage infiltration, tissue sections were incubated in phosphate-buffered saline plus 4% bovine serum albumin (Sigma) plus 0.1% Triton (BDH) and then in biotinylated antimouse/leukocyte common antigen CD45.2 monoclonal antibody (mAb) (clone 104; BD Pharmingen) or antimouse CD68 mAb (FA-11; Serotec). Signals were revealed with R.T.U. horseradish peroxidase streptavidin (Vector Laboratories), which was detected using a Vector NovaRED substrate kit (Vector Laboratories). Slides were counterstained with Mayer hematoxylin and examined under an Eclipse 55i microscope (Nikon). Images were captured with Digital Sight DS-5 M digital camera (Nikon) using Lucia G software (Laboratory Imaging). Parallel slides in which the primary mAb had been omitted were identically processed and used as negative controls. Stained sections were examined by 3 independent operators masked to experimental design.

To verify the efficacy of the macrophage depletion, peritoneal fluid was retrieved at various time points and analyzed by flow cytometry. Samples were incubated for 10 min at room temperature with phosphate-buffered saline containing 10% fetal bovine serum. Phycoerythrin-conjugated anti-F4/80 mAb (clone CI: A3-1; SeroTec) was added for 20 min. Red blood cell lysis buffer (NH_4Cl [0.15 M/L], $KHCO_3$ [1 mmol/L], and Na_2EDTA [0.1 mmol/L]) was added for 10 min at room temperature before analysis (FACS Calibur flow cytometer and CellQuest software; BD Biosciences).

Viability In Vitro Assays

The constant number of TS/A adenocarcinoma cells was challenged in vitro with increasing amounts of liposomes containing or not containing clodronate (5, 20, and 40 μL of Clodrolip or Shamlip suspensions per milliliter). Sixteen hours afterward, supernatants were collected for freezing and cells were harvested. Apoptotic cells were identified by flow cytometry using the Annexin V-FITC Apoptosis Detection Kit (Immunostep Research, Valter Occhiena) according to the manufacturer's instructions. Cytometric analysis was performed using a FACS Calibur (BD Biosciences) and the Cell Quest software (BD Biosciences). Data were analyzed with FCS Express software (BD Biosciences). In parallel, the concentration of lactate dehydrogenase in the supernatants was measured using the CytoTox-ONE™ Homogeneous Membrane Integrity Assay (Promega). Analysis was performed using a Victor3 Wallac (1420 Multilabel Counter; Perkin Elmer) according to manufacturer's instructions. As a positive control of necrosis, the supernatant of adenocarcinoma cells lysed in the presence of Triton X100 nonionic detergent (1%) was used.

Statistical Analysis

Results are expressed as mean ± SD. Experimental differences were tested for statistical significance using a Student t test (unpaired, 2-sided, P considered statistically significant when < 0.05) and Prism (version 4.0c [GraphPad Software] for Macintosh [Software MacKiev]). Correlation was calculated with a Pearson test (2-tailed, 95% confidence interval) using Prism software, and linear regression was also calculated using Prism.

RESULTS

Experimental Model of Peritoneal Carcinomatosis and ^{18}F-FDG Distribution

To evaluate the feasibility of using ^{18}F-FDG PET in monitoring onset and progression of experimental peritoneal carcinomatosis, we set up a model based on the intraperitoneal injection of syngeneic murine TS/A adenocarcinoma cells in BALB/C female mice. TS/A adenocarcinoma is a spontaneous tumor cell line arisen in BALB/C female retired breeders and expanded in vitro (*13*). The model nicely recapitulated the histologic features of the human disease: adenocarcinoma cells distributed along the cavity and yielded several 3-dimensional masses attached to the peritoneal lining. In 1 week, animals developed masses with a microscopic architecture typical of adenocarcinoma lesions, with cribriformlike structures (Supplemental Fig. 1A; supplemental materials are available online only at http://jnm.snmjournals.org), characterized by scant vascularization and a large infiltration of macrophages (data not shown).

We initially verified whether this model was suitable for an ^{18}F-FDG PET study. To this aim, we performed a model-setting pilot study by scanning mice at 4 and 10 d after TS/A adenocarcinoma cell injection. No evidence of disease was detectable at 4 d. At 10 d, intense spots of ^{18}F-FDG uptake inside the peritoneum were detectable in all animals. These areas corresponded to actual peritoneal neoplastic lesions, as verified at necropsy (Supplemental Fig. 1B).

Relative Contribution of Neoplastic Cells and Tumor-Associated Phagocytes to ^{18}F-FDG Uptake

We then studied parallel cohorts of TS/A adenocarcinoma–bearing mice either depleted of peritoneal macrophages with Clodrolip or sham-treated (Fig. 1). Peritoneal macrophage depletion, evaluated by staining peritoneal cells for the F4/80 macrophage marker, was routinely between 46.5% and 97.9% (Supplemental Fig. 2A). Depletion was confirmed in tumor tissues by staining for the CD68 macrophage marker (Supplemental Fig. 2B). Clodrolip did not have direct cytotoxic effects on TS/A adenocarcinoma cells, because it did not cause the exposure of anionic phospholipids

on the outer plasma membrane, an early event in programmed cell death via apoptosis (Supplemental Figs. 2C and 2D), or the release of the enzyme lactate dehydrogenase (Supplemental Fig. 2E) indicative of primary or postapoptotic necrosis.

We monitored disease progression in macrophage-competent or -depleted animals with ^{18}F-FDG PET in a longitudinal PET study at 5, 7, 9, and 12 d after TS/A adenocarcinoma cell injection (Figs. 2A and 2B). At 7 d after TS/A adenocarcinoma cells injection, neoplastic lesions in control mice displayed high ^{18}F-FDG uptake. Scattered positive spots of ^{18}F-FDG rapidly increased in intensity and extent thereafter, from day 9 to day 12 (Fig. 2A). Macrophages influenced both tumor growth and ^{18}F-FDG distribution: indeed in macrophage-depleted mice, we did not detect any relevant uptake at 7 and 9 d. Only at later time points (12 d) could some defined signals be identified in macrophage-depleted mice (Fig. 2B). In both cohorts of mice, radioactivity corresponded to actual neoplastic lesions, as observed by necropsy (Figs. 2A and 2B). The amount of ascites developed by the 2 groups was similar (data not shown).

We analyzed by immunohistochemistry the presence and relative proportion of inflammatory cells infiltrating peritoneal adenocarcinoma lesions in mice at 7 (early effect) and 12 d (late effect) after TS/A adenocarcinoma cell injection (Fig. 2C). The treatment with Clodrolip drastically reduced the inflammatory infiltrate both at early and at late time points (Fig. 2D). Radioactivity distribution obtained with ^{18}F-FDG PET corresponded to the location of lesions observed during necropsy (data not shown) also for the early time point, at 7 d after TS/A adenocarcinoma cell injection.

Quantification and Correlations Analysis

To better characterize the effects of macrophages on ^{18}F-FDG distribution we applied a quantitative analysis on ^{18}F-FDG PET images and correlated the results of ^{18}F-FDG PET image quantification with the weight of neoplastic lesions sampled postmortem.

Figure 3 shows a representative example of thresholded maps of radioactivity distribution and the correspondent PET images of representative mice. The tumor volume measured using ^{18}F-FDG PET (tumor PET volume) was significantly lower after macrophage depletion (0.64 ± 0.40 cm^3 vs. 0.17 ± 0.19 cm^3, $P < 0.005$; 0.87 ± 0.29 cm^3 vs. 0.13 ± 0.13 cm^3, $P < 0.0005$; and 1.31 ± 0.71 cm^3 vs. 0.53 ± 0.49 cm^3, $P = 0.01$, at 7, 9, and 12 d after TS/A adenocarcinoma cell injection in control and macrophage-depleted mice, respectively). At 12 d after TS/A adenocarcinoma cell injection, we observed an increase in the extent of PET tumor
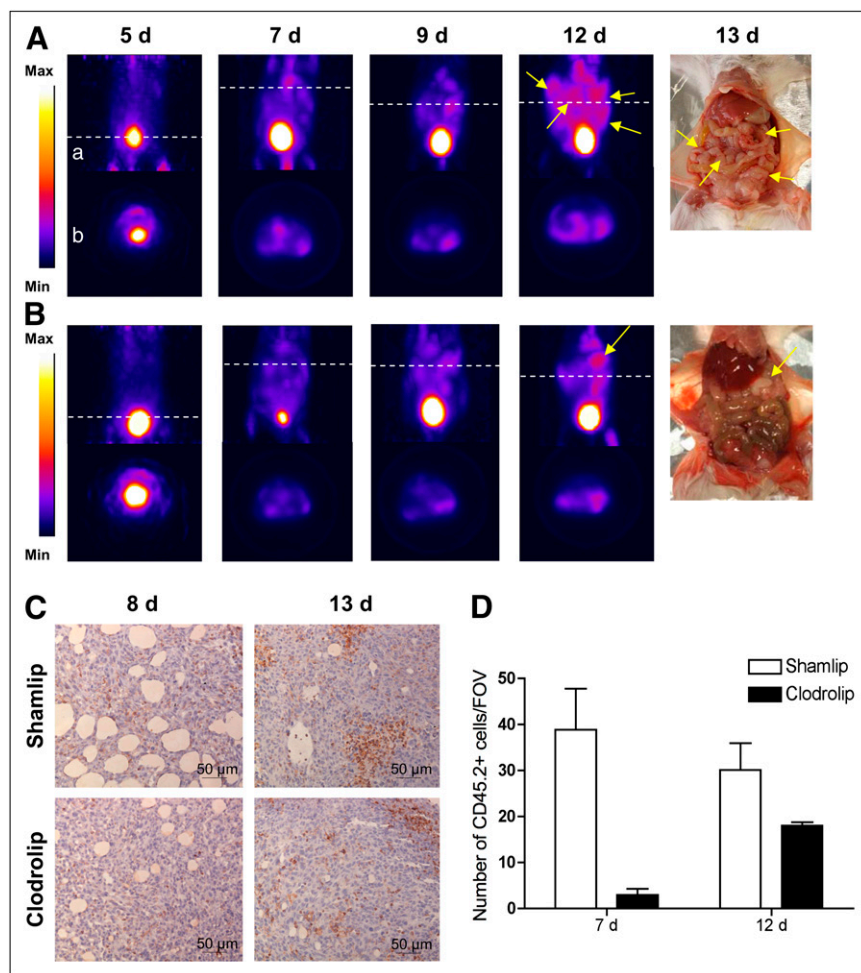
FIGURE 2. Relative contribution of neoplastic cells and macrophages to ^{18}F-FDG uptake. ^{18}F-FDG PET scans of abdomen of representative mice from Shamlip- (A) and Clodrolip (B)-treated cohorts at different time points. Coronal view (a) of image reconstruction and axial slices (b) taken at level of tumor location (dashed white line); right panels show pictures of scanned mice at moment of necropsy. Tumor masses are indicated by yellow arrows. (C) Immunohistochemical staining for CD45.2 of neoplastic lesions from representative Shamlip- and Clodrolip-treated animals, at early (8 d) and late (13 d) time points. (D) Quantification of number of CD45.2-positive cells infiltrating tumor lesions per FOV (×20); results are expressed as mean of counts of 4 fields per tumor mass per animal. One animal per experimental condition per group was analyzed, from 3 independent experiments. Max = maximum; Min = minimum.

volume in macrophage-depleted animals (Fig. 3). At this time point, leukocyte infiltration was slightly increased, though still limited (Fig. 2D): the gain in tumor PET volume thus possibly depends on macrophage-independent events.

Mean values of maximum ^{18}F-FDG uptake in thresholded tumor regions, expressed as maximum SUV, were significantly lower in macrophage-depleted mice if compared with control Shamlip-treated mice. The greatest difference was observed at 9 d, after TS/A adenocarcinoma cell injection (Fig. 4, $P = 0.002$), when the tumor volume was minimal.

The observed increase in tumor PET volume in macrophage-depleted mice from 7 to 12 d was also confirmed by the quantification of maximum ^{18}F-FDG uptake (Fig. 4; *$P < 0.05$). However, unlike what was observed for tumor PET volume, radioactivity concentration expressed as maximum ^{18}F-FDG uptake was only slightly reduced by Clodrolip treatment, with the exception of the 9-d time point. Interestingly, the maximum ^{18}F-FDG uptake signal observed at 7 d in depleted animals was independent of phagocyte accumulation (Fig. 2 D), indicating that the major role in the level of ^{18}F-FDG uptake was played by neoplastic cells. Similar results were also obtained for mean SUV: ^{18}F-FDG uptake was significantly lower at 9 d (data not shown).

Moreover, we directly measured tumor load by weighting lesions harvested from macrophage-depleted and -competent animals. Macrophage depletion was associated with a substantially smaller tumor burden 13 d after TS/A adenocarcinoma cell injection than in sham-treated mice (Fig. 5A). This observation confirmed the trend shown with ^{18}F-FDG PET scan analysis and is in agreement with the established trophic action of macrophages. A partial reduction in neoplastic load was also observed at an earlier time point (7 d) in macrophage-depleted mice (Fig. 5C). In addition, the weight of lesions positively correlated with the extent of radioactivity uptake measured in vivo using ^{18}F-FDG PET, both at 7 and at 12 d after TS/A adenocarcinoma cell injection (Figs. 5D and 5B, respectively).

DISCUSSION

Most preclinical studies for peritoneal carcinomatosis have been conducted on xenograft models that rely on human cancer cells transferred into immunodeficient mice (17), which do not fully reproduce the environment of peritoneal carcinomatosis (18). Here, we have established an ad hoc murine model of aggressive peritoneal carcinomatosis based on the injection of murine TS/A adenocarcinoma cells in the peritoneum of syngeneic mice. TS/A cells were derived from a spontaneous mammary adenocarcinoma that arose in a BALB/C mouse (13). The liver, lungs, and bones are the most common sites of breast cancer metastases (19). Breast cancer, however, shares with gastrointestinal carcinomas the potential to metastasize to the lower genital tract and to spread to the peritoneal lining (20). Our model well reproduces the main clinical histologic features of peritoneal lesions derived from adenocarcinoma of various origins in terms of architecture, angiogenesis, abundance, and characteristics of infiltrating inflammatory cells.

We have characterized the role of macrophages in live animals using ^{18}F-FDG PET. The results demonstrate the feasibility of preclinical approaches for the imaging and study of inaccessible sites, such as the abdominal cavity (Supplemental Fig. 1).

To address the role of a single nonneoplastic constituent of peritoneal lesions, macrophages, in tumor growth and in the generation of ^{18}F-FDG PET signal, we compared neoplastic lesion extent, histologic features, and ^{18}F-FDG PET in Shamlip-treated, macrophage-competent and Clodrolip-treated, macrophage-depleted mice. Clodronate, a drug used in clinical practice to treat bone dysfunctions, when encapsulated in artificial lipid spheres (liposomes) is internalized
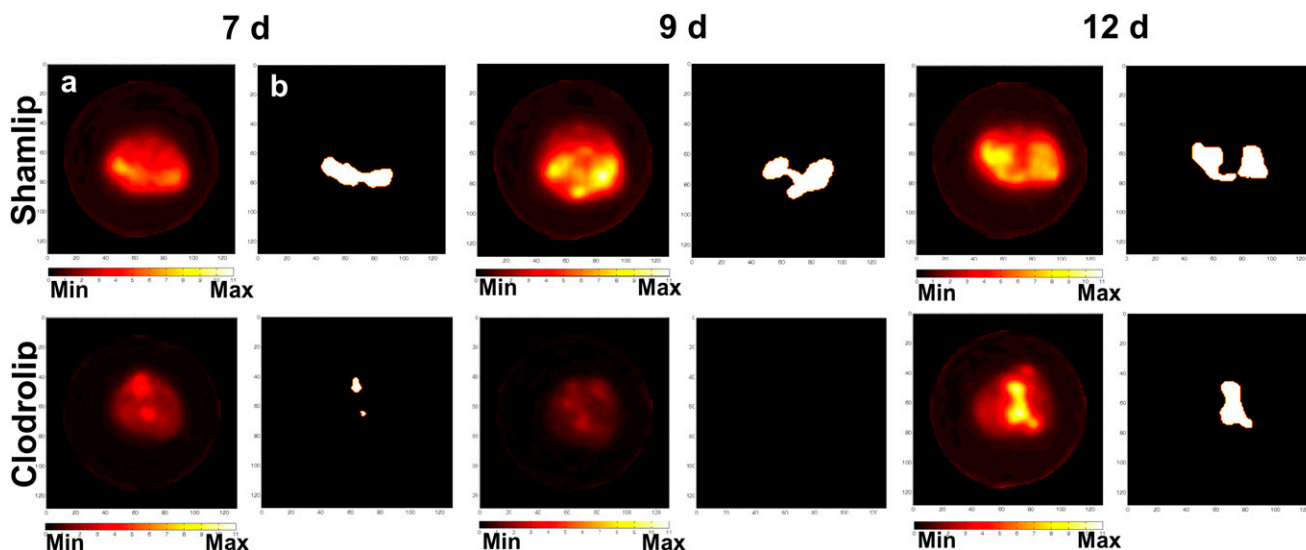
FIGURE 3. Quantitative analysis. Axial ^{18}F-FDG PET scans (a) and reelaborated images with tumor contour masks (b) of 2 representative mice from Shamlip- (upper) and Clodrolip (lower)-treated cohorts, at different time points. Max = maximum; Min = minimum.
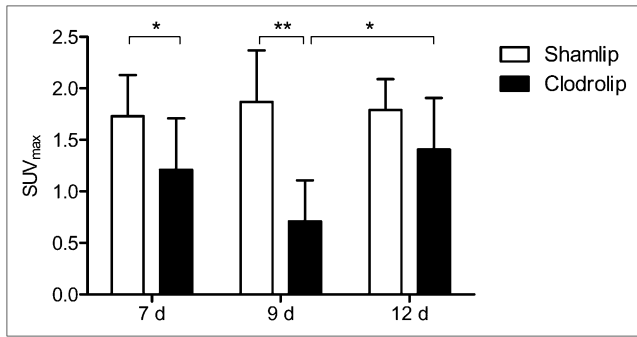
FIGURE 4. Variation of maximum ^{18}F-FDG uptake (expressed as SUV) during time in Shamlip- and Clodrolip-treated cohorts of mice. Error bars represent SD of 2 independent experiments for 7 ($n = 9$ for Shamlip and $n = 11$ for Clodrolip) and 12 d ($n = 10$ for each group) and 1 experiment for 9 d ($n = 5$ for Shamlip and $n = 6$ for Clodrolip). SUV_{max} = maximum SUV.

more effectively (*14*) and represents an effective method of eliminating phagocytes in preclinical settings in vivo (*21*). Liposomes are ingested by macrophages with high efficiency, and apoptosis is eventually induced, possibly via modulation of intracellular iron and calcium homeostasis (*22*) or of adenosine triphosphate metabolism (*23*). This approach allows the elimination of resident and infiltrating macrophages in various organs depending on the administration route (*24*). Here, we observed that macrophages are necessary for lesion growth (Fig. 5). Lesion weight and PET tumor volume were concomitantly decreased in animals treated with Clodrolip at 7 and 9 d after TS/A cell injection, followed by a slight increase in PET tumor volume at 12 d. The latter event suggests a tumor escape mechanism, relying on macrophage-independent pathways. At that time, we ob-

served also a partial restoration of inflammatory infiltrate (Fig. 2D). TAMs promote tissue remodeling and neovascularization (*25,26*), because they can be educated by neoplastic cells to support tumor progression and metastasis (*27*). In our model, their action is apparently nonredundant at earlier time points. At later phases, other stromal sources of angiogenetic or tumorigenic signals, such as mast cells, neutrophils, fibroblasts, or dendritic cells, may sustain tumor growth (*28*).

The metabolic activity of lesions was only minimally modified by Clodrolip treatment (Fig. 4), with the exception of the 9-d time point, when partial-volume effects only influence the quantification of the radioactivity concentration. In addition, the relative presence of inflammatory infiltrate within the lesion does not affect per se ^{18}F-FDG uptake, as indicated by the lack of differences in maximum ^{18}F-FDG uptake found at 7 d (with minimal residual inflammatory CD45.2^{+}-infiltrating cells, 2.88 ± 2.34/FOV) and at day 12 (with a 6-fold increase of CD45.2^{+}-infiltrating cells, 18.02 ± 1.28/FOV).

Several biochemical events possibly contribute to the uptake of ^{18}F-FDG in neoplastic lesions. Transformed cells are characterized by the aberrant expression of membrane glucose transporters (*29*), with an increased glycolytic metabolism even in aerobic conditions (*30,31*). However, phagocytes are also effective accumulators of ^{18}F-FDG because of their constitutively high endocytic activity (*32*). The accumulation of inflammatory cells is often associated with false-positive results in ^{18}F-FDG PET–based studies (*33–35*), and both the number and the activation state of inflammatory cells have been demonstrated to contribute to the ^{18}F-FDG uptake at preclinical and clinical level (*36,37*).
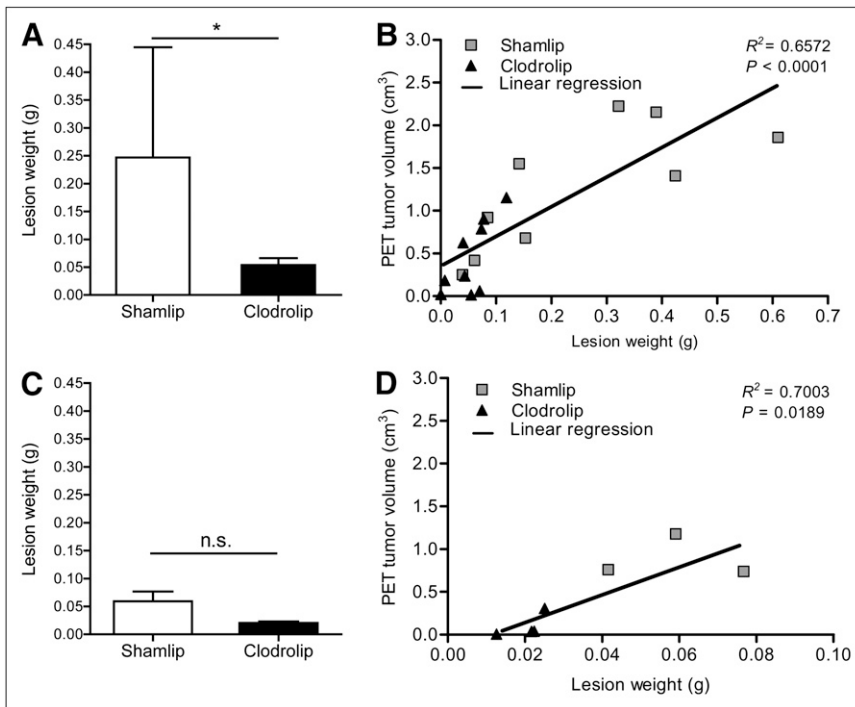
FIGURE 5. PET information strongly correlates with necropsy. (A) Lesion weight from Shamlip- and Clodrolip-treated cohorts of mice at 12 d after TS/A cell injection. Error bars are SD; $n = 9$ each cohort from 2 independent experiments. (B) Correlation plot between lesion weight (*x*-axis) and volume of tumor measured at PET (*y*-axis) of tumors of Shamlip- and Clodrolip-treated mice at 12 d after TS/A cell injection; $n = 9$ from 2 independent experiments. Linear regression curve considers both cohorts. Correlation value is $r = 0.8107$. (C) Lesion weight from Shamlip- and Clodrolip-treated cohorts of mice at 7 d after TS/A cell injection. Error bars are SD; $n = 4$ for Clodrolip and $n = 3$ for Shamlip. (D) Correlation plot between lesion weight (*x*-axis) and volume of tumor measured by PET (*y*-axis) of tumors of Shamlip- and Clodrolip-treated mice at 7 d. Linear regression curve considers both cohorts. Correlation value is $r = 0.8368$. *$P < 0.05$.

We observed that the extent of PET signal correlates with lesion weight, merging data deriving from mice with various levels of macrophages (Clodrolip- or Shamlip-treated, Clodrolip-treated mice at day 12), and the metabolic phenotype of lesions does not change substantially, even when the tumor is virtually depleted of macrophages. Thus, neoplastic cells represent the major player in the imaging results in vivo, as is particularly evident at later time points after depletion (Fig. 4; day 12), when tumors, although still devoid of macrophages, consistently grow and take up ^{18}F-FDG. A contribution of metabolically active inflammatory cells to the generation of ^{18}F-FDG PET signals cannot be completely excluded, particularly in sham-treated mice in which TAMs are not a confounding factor and actually participate to tumor growth. Increasing efforts should be dedicated to the development of specific probes, which could be valuable to further dissecting the role played by the various immune cells infiltrating neoplastic lesions, such as the radioligand for the deoxycytidine salvage pathway ^{18}F-FAC recently applied for the in vivo monitoring of CD8+ T cells in a tumor model (38).

Finally, our results suggest that TAM depletion represents a potential adjuvant strategy for ascitogenic tumors. Macrophages play a role in the response to paclitaxel in a breast cancer model (39), in which the enhanced inflammatory response due to the treatment and to the elicited cytotoxicity fuels macrophage actions. It is likely that the differentiation state of TAMs is critical: for instance a shift in the functional polarization from alternatively activated to classically activated macrophages leads to an opposite protective response against vascularized nonneoplastic endometrial lesions (10). Approaches aimed at redirecting TAM functions in vivo are being actively investigated (40).

CONCLUSION

Our results demonstrate that cancer cells represent the major contributor in ^{18}F-FDG uptake and confirm the pivotal role of macrophages in neoplastic peritoneal lesions growth and spreading (Supplemental Fig. 3).

DISCLOSURE STATEMENT

The costs of publication of this article were defrayed in part by the payment of page charges. Therefore, and solely to indicate this fact, this article is hereby marked "advertisement" in accordance with 18 USC section 1734.

REFERENCES

1. Kunisaki C, Akiyama H, Nomura M, et al. Comparison of surgical results of D2 versus D3 gastrectomy (para-aortic lymph node dissection) for advanced gastric carcinoma: a multi-institutional study. *Ann Surg Oncol.* 2006;13:659–667.
2. D'Angelica M, Gonen M, Brennan MF, Turnbull AD, Bains M, Karpeh MS. Patterns of initial recurrence in completely resected gastric adenocarcinoma. *Ann Surg.* 2004;240:808–816.
3. Sugarbaker PH, Yu W, Yonemura Y. Gastrectomy, peritonectomy, and perioperative intraperitoneal chemotherapy: the evolution of treatment strategies for advanced gastric cancer. *Semin Surg Oncol.* 2003;21:233–248.
4. Margolis DJ, Hoffman JM, Herfkens RJ, Jeffrey RB, Quon A, Gambhir SS. Molecular imaging techniques in body imaging. *Radiology.* 2007;245:333–356.
5. Iagaru AH, Mittra ES, McDougall IR, Quon A, Gambhir SS. ^{18}F-FDG PET/CT evaluation of patients with ovarian carcinoma. *Nucl Med Commun.* 2008;29:1046–1051.
6. Kim TJ, Ravoori M, Landen CN, et al. Antitumor and antivascular effects of AVE8062 in ovarian carcinoma. *Cancer Res.* 2007;67:9337–9345.
7. Zavaleta CL, Goins BA, Bao A, McManus LM, McMahan CA, Phillips WT. Imaging of [186]Re-liposome therapy in ovarian cancer xenograft model of peritoneal carcinomatosis. *J Drug Target.* 2008;16:626–637.
8. Nishiyama Y, Yamamoto Y, Kanenishi K, et al. Monitoring the neoadjuvant therapy response in gynecological cancer patients using FDG PET. *Eur J Nucl Med Mol Imaging.* 2008;35:287–295.
9. Mantovani A, Sica A, Allavena P, Garlanda C, Locati M. Tumor-associated macrophages and the related myeloid-derived suppressor cells as a paradigm of the diversity of macrophage activation. *Hum Immunol.* 2009;70:325–330.
10. Bacci M, Capobianco A, Monno A, et al. Macrophages are alternatively activated in patients with endometriosis and required for growth and vascularization of lesions in a mouse model of disease. *Am J Pathol.* 2009;175:547–556.
11. Kawamura K, Komohara Y, Takaishi K, Katabuchi H, Takeya M. Detection of M2 macrophages and colony-stimulating factor 1 expression in serous and mucinous ovarian epithelial tumors. *Pathol Int.* 2009;59:300–305.
12. Pollard JW. Tumour-educated macrophages promote tumour progression and metastasis. *Nat Rev Cancer.* 2004;4:71–78.
13. Nanni P, de Giovanni C, Lollini PL, Nicoletti G, Prodi G. TS/A: a new metastasizing cell line from a BALB/c spontaneous mammary adenocarcinoma. *Clin Exp Metastasis.* 1983;1:373–380.
14. Van Rooijen N, Sanders A. Liposome mediated depletion of macrophages: mechanism of action, preparation of liposomes and applications. *J Immunol Methods.* 1994;174:83–93.
15. Motta A, Damiani C, Del Guerra A, Di Domenico G, Zavattini G. Use of a fast EM algorithm for 3D image reconstruction with the YAP-PET tomograph. *Comput Med Imaging Graph.* 2002;26:293–302.
16. ImageJ. Available at: http://rsbweb.nih.gov/ij/. Accessed September 29, 2011.
17. Fong MY, Kakar SS. Ovarian cancer mouse models: a summary of current models and their limitations. *J Ovarian Res.* 2009;2:12.
18. Brown RS, Fisher SJ, Wahl RL. Autoradiographic evaluation of the intra-tumoral distribution of 2-deoxy-D-glucose and monoclonal antibodies in xenografts of human ovarian adenocarcinoma. *J Nucl Med.* 1993;34:75–82.
19. Hüsemann Y, Geigl JB, Schubert F, et al. Systemic spread is an early step in breast cancer. *Cancer Cell.* 2008;13:58–68.
20. Engelstaedter V, Mylonas I. Lower genital tract metastases at time of first diagnosis of mammary invasive lobular carcinoma. *Arch Gynecol Obstet.* 2011;283 (suppl 1:93–95.
21. van Rooijen N. Liposomes for targeting of antigens and drugs: immunoadjuvant activity and liposome-mediated depletion of macrophages. *J Drug Target.* 2008;16:529–534.

22. Mönkkönen J, Heath TD. The effects of liposome-encapsulated and free clodronate on the growth of macrophage-like cells in vitro: the role of calcium and iron. *Calcif Tissue Int.* 1993;53:139–146.

23. van Rooijen N. Extracellular and intracellular action of clodronate in osteolytic bone diseases? A hypothesis. *Calcif Tissue Int.* 1993;52:407–410.

24. Buiting AM, Zhou F, Bakker JA, van Rooijen N, Huang L. Biodistribution of clodronate and liposomes used in the liposome mediated macrophage 'suicide' approach. *J Immunol Methods.* 1996;192:55–62.

25. Gordon S. Alternative activation of macrophages. *Nat Rev Immunol.* 2003;3:23–35.

26. Mosser DM, Edwards JP. Exploring the full spectrum of macrophage activation. *Nat Rev Immunol.* 2008;8:958–969.

27. Coffelt SB, Hughes R, Lewis CE. Tumor-associated macrophages: effectors of angiogenesis and tumor progression. *Biochim Biophys Acta.* 2009;1796:11–18.

28. Mantovani A, Sica A. Macrophages, innate immunity and cancer: balance, tolerance, and diversity. *Curr Opin Immunol.* 2010;22:231–237.

29. Macheda ML, Rogers S, Best JD. Molecular and cellular regulation of glucose transporter (GLUT) proteins in cancer. *J Cell Physiol.* 2005;202:654–662.

30. Vander Heiden MG, Cantley LC, Thompson CB. Understanding the Warburg effect: the metabolic requirements of cell proliferation. *Science.* 2009;324:1029–1033.

31. DeBerardinis RJ, Lum JJ, Hatzivassiliou G, Thompson CB. The biology of cancer: metabolic reprogramming fuels cell growth and proliferation. *Cell Metab.* 2008;7:11–20.

32. Kubota R, Yamada S, Kubota K, Ishiwata K, Tamahashi N, Ido T. Intratumoral distribution of fluorine-18-fluorodeoxyglucose in vivo: high accumulation in macrophages and granulation tissues studied by microautoradiography. *J Nucl Med.* 1992;33:1972–1980.

33. Brewer S, McPherson M, Fujiwara D, et al. Molecular imaging of murine intestinal inflammation with 2-deoxy-2-[^{18}F]fluoro-D-glucose and positron emission tomography. *Gastroenterology.* 2008;135:744–755.

34. Rosenbaum SJ, Lind T, Antoch G, Bockisch A. false-positive FDG PET uptake: the role of PET/CT. *Eur Radiol.* 2006;16:1054–1065.

35. Yamada S, Kubota K, Kubota R, Ido T, Tamahashi N. High accumulation of fluorine-18-fluorodeoxyglucose in turpentine-induced inflammatory tissue. *J Nucl Med.* 1995;36:1301–1306.

36. Brepoels L, Stroobants S, Vandenberghe P, et al. Effect of corticosteroids on ^{18}F-FDG uptake in tumor lesions after chemotherapy. *J Nucl Med.* 2007;48:390–397.

37. Zhuang H, Pourdehnad M, Lambright ES, et al. Dual time point ^{18}F-FDG PET imaging for differentiating malignant from inflammatory processes. *J Nucl Med.* 2001;42:1412–1417.

38. Nair-Gill E, Wiltzius SM, Wei XX, et al. PET probes for distinct metabolic pathways have different cell specificities during immune responses in mice. *J Clin Invest.* 2010;120:2005–2015.

39. DeNardo DG. Leukocyte complexity predicts breast cancer survival and functionally regulates response to chemotherapy. *Cancer Discovery.* 2011;1:52–65.

40. Qian BZ, Pollard JW. Macrophage diversity enhances tumor progression and metastasis. *Cell.* 2010;141:39–51.